ISSN 1674-1056
http://cpb.iphy.ac.cn
http://iopscience.iop.org/cpb
中国物理 B
Chinese Physics
中国物理 Chinese Physics B

Noise properties of multi-combination information in x-ray grating-based phase-contrast imaging

Wali Faiz[1], Ji Li(李冀)[1], Kun Gao(高昆)[2], Zhao Wu(吴朝)[2], Yao-Hu Lei(雷耀虎)[1], Jian-Heng Huang(黄建衡)[1], Pei-Ping Zhu(朱佩平)[3,4]

Citation: Chin. Phys. B . 2020, 29(1): 014301 . **doi:** 10.1088/1674-1056/ab5780
Journal homepage: http://cpb.iphy.ac.cn; http://iopscience.iop.org/cpb

What follows is a list of articles you may be interested in

Implication of two-coupled tri-stable stochastic resonance in weak signal detection

Quan-Quan Li(李泉泉), Xue-Mei Xu(许雪梅), Lin-Zi Yin(尹林子), Yi-Peng Ding(丁一鹏), Jia-Feng Ding(丁家峰), Ke-Hui Sun(孙克辉)

Chin. Phys. B . 2018, 27(3): 034203 . **doi:** 10.1088/1674-1056/27/3/034203

Wavefront modulation of water surface wave by a metasurface

Sun Hai-Tao, Cheng Ying, Wang Jing-Shi, Liu Xiao-Jun

Chin. Phys. B . 2015, 24(10): 104302 . **doi:** 10.1088/1674-1056/24/10/104302

Theory of noise in a kilo-Hz cascaded high-energy Yb-doped nanosecond pulsed fiber amplifier

Liu Ming, Zhang Hai-Tao, Gong Ma-Li, Zhao Yue-Jin, Cheng Wen-Yong, Meng Kuo, Zheng Chao, Chen Yi-Zhu

Chin. Phys. B . 2014, 23(4): 044214 . **doi:** 10.1088/1674-1056/23/4/044214

Nonvolatile photorefractive properties in triply doped stoichiometric Mg：Fe：Mn：$LiTaO_3$ crystals

Sun Ting, Zhang Xiao-Dong, Sun Liang, Wang Rui

Chin. Phys. B . 2014, 23(1): 014204 . **doi:** 10.1088/1674-1056/23/1/014204

A modified phase diversity wavefront sensor with a diffraction grating

Luo Qun, Huang Lin-Hai, Gu Nai-Ting, Rao Chang-Hui

Chin. Phys. B . 2012, 21(9): 094201 . **doi:** 10.1088/1674-1056/21/9/094201

Noise properties of multi-combination information in x-ray grating-based phase-contrast imaging*

Wali Faiz[1], Ji Li(李冀)[1], Kun Gao(高昆)[2], Zhao Wu(吴朝)[2],
Yao-Hu Lei(雷耀虎)[1,†], Jian-Heng Huang(黄建衡)[1,‡], and Pei-Ping Zhu(朱佩平)[3,4]

[1] *Key Laboratory of Optoelectronic Devices and Systems of Ministry of Education and Guangdong Province, College of Physics and Optoelectronic Engineering, Shenzhen University, Shenzhen* 518060, *China*
[2] *National Synchrotron Radiation Laboratory, University of Science and Technology of China, Hefei* 230029, *China*
[3] *Institute of High Energy Physics, Chinese Academy of Sciences, Beijing* 100049, *China*
[4] *University of Chinese Academy of Sciences, Beijing* 100049, *China*

(Received 17 September 2019; revised manuscript received 18 October 2019; accepted manuscript online 14 November 2019)

Grating-based x-ray phase contrast imaging has attracted increasing interest in recent decades as multimodal and laboratory source usable method. Specific efforts have been focused on establishing a new extraction method to perform practical applications. In this work, noise properties of multi-combination information of newly established information extraction method, so-called angular signal radiography method, are investigated to provide guidelines for targeted and specific applications. The results show that how multi-combination of images can be used in targeted practical applications to obtain a high-quality image in terms of signal-to-noise ratio. Our conclusions can also hold true for upcoming targeted practical applications such as biomedical imaging, non-destructive imaging, and materials science.

Keywords: grating-based phase-contrast imaging, signal-to-noise ratio, refraction, scattering

PACS: 42.30.Rx, 43.60.Cg, 42.25.Gy, 52.25.Os **DOI:** 10.1088/1674-1056/ab5780

1. Introduction

X-ray imaging is a widely used technique to examine inner structure of opaque materials. X-rays can be used to detect, identify or diagnose the objects without invasion in fields like security, non-destructive testing or medicine. However, absorption-based x-ray imaging suffer a limited contrast to low Z elements. Phase shift x-ray imaging techniques could give solution to this shortfall. In the hard x-ray energy range (10 keV–100 keV), the real part of complex index of refraction (associated with phase shift) is about 100–1000 times higher than imaginary part (associated with absorption). Moreover, its dependence of atomic number is weaker for real part of index of refraction than for imaginary part.[1] This means that low Z elements can present a better image by employing phase-shifting techniques. Besides, scattering imaging provides complementary and in-accessible information compared to absorption-based imaging. Scattering imaging discloses structure information on a submicron scale below spatial resolution of imaging system which is in-accessible by absorption and phase contrast signals, without using high-resolution detectors.[2–12]

In the past years, various methods have been developed to measure the phase shift of x-rays, including interferometric imaging,[13,14] propagation-based imaging,[15,16] and analyzer-based imaging.[17–20] Among these methods the grating-based x-ray phase-contrast imaging (GBPCI) has potential in image processing and medical applications due to its compatibility with laboratory x-ray along with synchrotron source.[21] However, the extraction methods are important in GBPCI for minimizing the radiation dose. In GBPCI, several information extraction methods have been proposed to separate absorption, refraction, and scattering signals from projection images. Phase-stepping (PS)[22] is widely used extraction method, but its discontinuous image acquisition restricts its clinical applications. On the other hand, reverse projection (RP)[23] is fast, simple, and low in dose, but is unable to extract scattering information. Angular signal radiography (ASR),[24] has improved the image acquisition speed and reduced overall radiation dose.

Noise is one of the important factors influencing the properties of the imaging system. Therefore, noise analysis of PS,[25–27] RP,[28] and ASR[29] methods have been proposed. However, to the best of our knowledge, there has been no noise analysis of multi images in GBPCI. Hence, the present work is to study the noise characteristics of multi-combination information in GBPCI by employing ASR. Our proposed noise

*Project supported by the National Natural Science Foundation of China (Grant No. 11535015), the National Special Foundation of China for Major Science Instrument (Grant No. 61227802), the National Natural Science Foundation of China (Grant Nos. 61405120, 61605119, 61571305, and 11674232), the Natural Science Foundation of Shenzhen, China (Grant No. JCYJ20170302142617703), and the Natural Science Foundation of Shenzhen University, China (Grant Nos. 2017017 and 2018041). The author (Faiz Wali) was sponsored by the Post-doctoral International Exchange Program of China.

†Corresponding author. E-mail: leiyaohu@szu.edu.cn
‡Corresponding author. E-mail: xianhuangjianheng@163.com

© 2020 Chinese Physical Society and IOP Publishing Ltd

analysis would be useful for targeted applications of GBPCI in various fields where absorption, refraction and/or scattering images or their combinations (so-called multi-combination information) are required.

2. Theory

According to classical imaging description, the detected image function can be obtained by taking the convolution of angle modulated function (AMF) and angular signal response function (ASRF). The AMF characterizes the object properties, like absorption, refraction, and scattering while ASRF represents the detected intensity in GBPCI system. In the sample-beam interactions the absorption, refraction, and scattering deviate incoming x-rays, that is, absorption causes zero angular signal, refraction produces angular signal, and scattering is associated with angular distribution signal. According to the above sample–beam interactions the AMF can be described as[24]

$$f(\psi;x,y) = I_0 \frac{\exp[-M(x,y)]}{\sqrt{2\pi}\upsilon_s(x,y)} \times \exp\left[-\frac{1}{2}\frac{(\psi-\theta(x,y))^2}{\upsilon_s^2(x,y)}\right], \quad (1)$$

where $M(x,y)$, $\theta(x,y)$, $\upsilon_s^2(x,y)$, I_0, and ψ are the absorption, refraction angle, scattering variance of sample, intensity of incident x-ray beam, and x-ray deviation angle respectively.

Grating-based Talbot interferometer schematic setup is shown in Fig. 1(a). It consists of x-ray source, a detector, a phase grating G1, an analyzer grating G2, and a rotational sample stage. In grating interferometer, G1 acts as an angular collimator, while G2 acts as an angular filter and is set at self-image distance D downstream of G1. When G2 is shifted by small displacement (x_g) with respect to G1 in the perpendicular direction of x-ray beam, then the detected intensity changes. The variation in detected intensity as a function of x_g is called shifting curve (SC) and is shown in Fig. 1(b).

Angular deviation (x_g/D) is produced in Talbot interferometer by shifting relative displacement between G1 and G2, so ASRF is substituted by SC and is given as

$$S(\psi) = S(x_g/D) = \overline{S}\left[1 - V_0\cos\left(\frac{2\pi D}{p}(\psi+\psi_0) + \eta\frac{\pi}{2}\right)\right], \quad (2)$$

where p is the period of G2, ψ_0 is the initial deviation angle, $\overline{S}$ is the mean value, V_0 is the visibility of background SC, and $\eta = 0,1,2,3$, which is the modulation parameter. SC can be fitted with a cosine curve.[30,31] Here, imaging data are investigated for four typical sections (valley-SC (V), upslope-SC (U), peak-SC (P), and downslope-SC (D)) on SC as shown in Fig. 1(b). When an object is placed in x-ray beam, the periodic intensity pattern changes, so by using Eqs. (1) and (2), the four typical imaging equations can be expressed as[24]

$$I_V^s(x,y) = I_0\overline{S}e^{-M(x,y)}[1 - V(x,y)\cos(\phi(x,y))], \quad (3)$$
$$I_U^s(x,y) = I_0\overline{S}e^{-M(x,y)}[1 + V(x,y)\sin(\phi(x,y))], \quad (4)$$
$$I_P^s(x,y) = I_0\overline{S}e^{-M(x,y)}[1 + V(x,y)\cos(\phi(x,y))], \quad (5)$$
$$I_D^s(x,y) = I_0\overline{S}e^{-M(x,y)}[1 - V(x,y)\sin(\phi(x,y))], \quad (6)$$

where $V(x,y) = V_0\exp\left[-2\pi^2D^2\upsilon_s^2(x,y)/p^2\right]$ and $\phi(x,y) = (2\pi D/p)(\theta(x,y)+\psi_0)$.

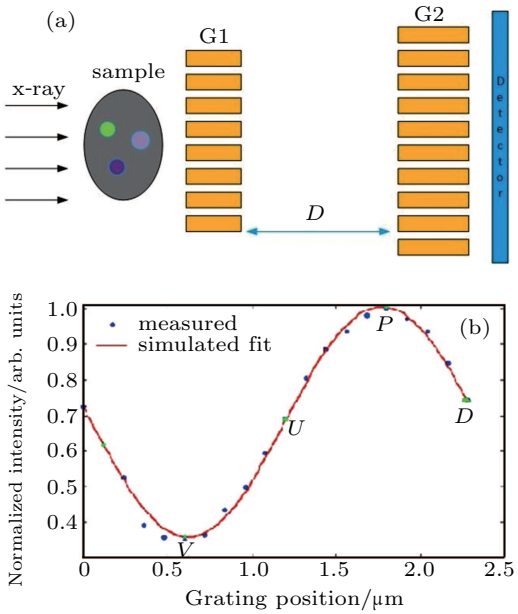


Fig. 1. (a) Schematic setup of GBPCI and (b) plot of SC *versus* grating position.

To eliminate ψ_0, the effective absorption, refraction, and scattering image of the object are calculated with and without sample in beam path at four typical points on SC. Then using Eqs. (3)–(6), the effective absorption, refraction angle, and scattering variance are extracted from (for simplicity (x,y) is omitted)

$$M = \ln\left[\frac{I_U^b + I_D^b}{I_U^s + I_D^s}\right], \quad (7)$$

$$\theta = -\frac{p}{2\pi D}\left[\arctan\left(\frac{I_U^s - I_D^s}{I_V^s - I_P^s}\right) - \arctan\left(\frac{I_U^b - I_D^b}{I_V^b - I_P^b}\right)\right], \quad (8)$$

$$\upsilon_s^2 = -\frac{p^2}{2\pi^2D^2}\ln\left[\frac{\sqrt{(I_U^s - I_D^s)^2 + (I_V^s - I_P^s)^2}}{V_0(I_U^s + I_D^s)}\right] + \frac{p^2}{2\pi^2D^2}\ln\left[\frac{\sqrt{(I_U^b - I_D^b)^2 + (I_V^b - I_P^b)^2}}{V_0(I_U^b + I_D^b)}\right], \quad (9)$$

where I_V^b, I_U^b, I_P^b, and I_D^b are the projection background images (without sample) while I_V^s, I_U^s, I_P^s, and I_D^s are the sample images at four typical positions (V, U, P, D) of SC.

In practical applications, only one or two sample-beam interactions may be required. In the case of low Z object, refraction and scattering information are prominent but absorption is negligible. In the case of edge investigation, the refraction information is significant and in the case of structural investigation, the scattering information is prominent. Here, by using ASR, multi-combinations of information and their noise are discussed in the next subsection.

2.1. Negligible scattering for ASR (NS-ASR)

If scattering information is neglected, *i.e.*, $\upsilon_{\rm s}^2(x,y)=0$, then by using Eqs. (4) and (6), the absorption and refraction information can be extracted from

$$M_{\rm NS} = \ln\left[\frac{I_U^{\rm b}+I_D^{\rm b}}{I_U^{\rm s}+I_D^{\rm s}}\right], \tag{10}$$

$$\theta_{\rm NS} = \frac{p}{2\pi D}\left[\arcsin\left(\frac{1}{V_0}\frac{I_D^{\rm s}-I_U^{\rm s}}{I_D^{\rm s}+I_U^{\rm s}}\right) - \arcsin\left(\frac{1}{V_0}\frac{I_D^{\rm b}-I_U^{\rm b}}{I_D^{\rm b}+I_U^{\rm b}}\right)\right]. \tag{11}$$

2.2. Negligible absorption for ASR (NA-ASR)

When absorption is negligible, *i.e.*, $M(x,y)=0$, then refraction and scattering information can be calculated by using Eqs. (3) and (6) and given as

$$\theta_{\rm NA} = \frac{p_2}{2\pi D}\left[\arctan\left(\frac{I_D^{\rm s}-I_0\bar{S}}{I_V^{\rm s}-I_0\bar{S}}\right) - \arctan\left(\frac{I_D^{\rm b}-I_0\bar{S}}{I_V^{\rm b}-I_0\bar{S}}\right)\right], \tag{12}$$

$$\upsilon_{\rm s,NA}^2 = \frac{p_2^2}{2\pi^2D^2}\ln\left[\frac{\sqrt{\left(I_D^{\rm b}-I_0\bar{S}\right)^2+\left(I_V^{\rm b}-I_0\bar{S}\right)^2}}{\sqrt{\left(I_D^{\rm s}-I_0\bar{S}\right)^2+\left(I_V^{\rm s}-I_0\bar{S}\right)^2}}\right]. \tag{13}$$

2.3. Negligible refraction for ASR (NR-ASR)

When refraction is negligible, *i.e.*, $\theta(x,y)=0$, then absorption and scattering information can be calculated by using Eqs. (3) and (5) and given as

$$M_{\rm NR} = \ln\left[\frac{I_V^{\rm b}+I_P^{\rm b}}{I_V^{\rm s}+I_P^{\rm s}}\right], \tag{14}$$

$$\upsilon_{\rm s,NR}^2 = \frac{p_2^2}{2\pi^2D^2}\ln\left[\frac{I_P^{\rm s}+I_V^{\rm s}}{I_P^{\rm s}-I_V^{\rm s}}\cdot\frac{I_P^{\rm b}+I_V^{\rm b}}{I_P^{\rm b}-I_V^{\rm b}}\right]. \tag{15}$$

2.4. Negligible absorption and refraction for ASR (NANR-ASR)

When absorption and refraction are both negligible, *i.e.*, $M(x,y)=\theta(x,y)=0$, then scattering information can be calculated by using Eq. (3) or Eq. (5) and given as

$$\upsilon_{\rm s,NANR}^2 = \frac{p_2^2}{2\pi^2D^2}\ln\left[\frac{I_P^{\rm b}-I_0\bar{S}}{I_P^{\rm s}-I_0\bar{S}}\right]. \tag{16}$$

2.5. Negligible absorption and scattering for ASR (NANS-ASR)

When both absorption and scattering are negligible, *i.e.*, $M(x,y)=\upsilon_{\rm s}^2(x,y)=0$, then refraction information can be calculated by using Eq. (4) or Eq. (6) and given as

$$\theta_{\rm NANS} = \frac{p_2}{2\pi D}\arcsin\left[\frac{I_U^{\rm s}-I_0\bar{S}}{V_0I_U^{\rm b}}\right]. \tag{17}$$

3. Noise analysis

In this section the photon statistical noise, one of the main factors affecting image quality, is discussed. Poisson statistics and error propagation[32] formula are used to derive noise.

3.1. Noise of NS-ASR

The noise in NS-ASR for absorption image is given as

$$\sigma_{M_{\rm NS}}^2 = \sum_{i=U,D}\left(\frac{\partial M_{\rm NS}}{\partial I_i^{\rm s}}\right)^2_{I_i^{\rm s}=\overline{I_i^{\rm s}}}\sigma_{I_i}^2.$$

By using Eqs. (4) and (6), we obtain

$$\sigma_{M_{\rm NS}}^2 = \frac{1}{2I_0\bar{S}{\rm e}^{-M}},$$

$${\rm SNR}_{M_{\rm NS}} = \sqrt{2I_0\bar{S}{\rm e}^{-M}}M.$$

The noise in NS-ASR for refraction image is given as

$$\sigma_{\theta_{\rm NS}}^2 = \sum_{i=U,D}\left(\frac{\partial\theta_{\rm NS}}{\partial I_i^{\rm s}}\right)^2_{I_i^{\rm s}=\overline{I_i^{\rm s}}}\sigma_{I_i}^2.$$

By using Eqs. (4) and (6), we have

$$\sigma_{\theta_{\rm NS}}^2 = \left(\frac{p}{2\pi D}\right)^2\frac{1-V_0^2\sin^2\phi}{2I_0\bar{S}{\rm e}^{-M}V_0^2\cos^2\phi},$$

$${\rm SNR}_{\theta_{\rm NS}} = \left(\frac{2\pi D}{p}\right)\frac{\sqrt{2I_0\bar{S}{\rm e}^{-M}}\theta V_0\cos\phi}{\sqrt{1-V_0^2\sin^2\phi}}.$$

3.2. Noise of NA-ASR

The noise in NA-ASR for refraction image is given as

$$\sigma_{\theta_{\rm NA}}^2 = \sum_{i=U,P}\left(\frac{\partial\theta_{\rm NA}}{\partial I_i^{\rm s}}\right)^2_{I_i^{\rm s}=\overline{I_i^{\rm s}}}\sigma_{I_i}^2.$$

By using Eqs. (3) and (6), we obtain

$$\sigma_{\theta_{\rm NA}}^2 = \left(\frac{p}{2\pi D}\right)^2\frac{1-V\sin\phi\cos\phi(\sin\phi+\cos\phi)}{I_0\bar{S}V^2},$$

$${\rm SNR}_{\theta_{\rm NA}} = \left(\frac{2\pi D}{p}\right)\frac{\sqrt{I_0\bar{S}}\theta V}{\sqrt{1-V\sin\phi\cos\phi(\sin\phi+\cos\phi)}}.$$

The noise in NA-ASR for scattering image is given as

$$\sigma_{\upsilon_{\rm sNA}^2}^2 = \sum_{i=U,P}\left(\frac{\partial\upsilon_{\rm sNA}^2}{\partial I_i^{\rm s}}\right)^2_{I_i^{\rm s}=\overline{I_i^{\rm s}}}\sigma_{I_i}^2.$$

By using Eqs. (3) and (6), we have

$$\sigma_{\upsilon_{\rm sNA}^2}^2 = \left(\frac{p^2}{2\pi^2D^2}\right)^2\frac{1-V(\sin^3\phi+\cos^3\phi)}{I_0\bar{S}V^2},$$

$${\rm SNR}_{\upsilon_{\rm sNA}^2} = \left(\frac{2\pi^2D^2}{p^2}\right)\frac{\sqrt{I_0\bar{S}V}\upsilon_{\rm s}^2}{\sqrt{1-V(\sin^3\phi+\cos^3\phi)}}.$$

3.3. Noise of NR-ASR

The noise in NR-ASR for absorption image is given as

$$\sigma^2_{M_{\rm NR}} = \sum_{i=V,P}\left(\frac{\partial M_{\rm NR}}{\partial I_i^{\rm s}}\right)^2_{I_i^{\rm s}=\overline{I_i^{\rm s}}}\sigma^2_{I_i}.$$

By using Eqs. (4) and (5), we have

$$\sigma^2_{M_{\rm NR}} = \frac{1}{2I_0\bar{S}{\rm e}^{-M}},$$

$$\mathrm{SNR}_{M_{\rm NR}} = \sqrt{2I_0\bar{S}{\rm e}^{-M}}M.$$

The noise in NR-ASR for scattering image is given as

$$\sigma^2_{\upsilon^2_{\rm sNR}} = \sum_{i=V,P}\left(\frac{\partial \upsilon^2_{\rm sNR}}{\partial I_i^{\rm s}}\right)^2_{I_i^{\rm s}=\overline{I_i^{\rm s}}}\sigma^2_{I_i},$$

$$\sigma^2_{\upsilon^2_{\rm sNR}} = \left(\frac{p^2}{2\pi^2D^2}\right)^2\frac{1-V^2}{2I_0\bar{S}{\rm e}^{-M}V^2},$$

$$\mathrm{SNR}_{\upsilon^2_{\rm sNR}} = \left(\frac{2\pi^2D^2}{p^2}\right)\frac{\sqrt{2I_0\bar{S}{\rm e}^{-M}V}\upsilon_{\rm s}^2}{\sqrt{1-V^2}}.$$

3.4. Noise of NANR-ASR

The noise in NANR-ASR is given as

$$\sigma^2_{\upsilon^2_{\rm sNANR}} = \left(\frac{\partial \upsilon^2_{\rm sNR}}{\partial I_P^{\rm s}}\right)^2_{I_i^{\rm s}=\overline{I_P^{\rm s}}}\sigma^2_{I_P},$$

$$\sigma^2_{\upsilon^2_{\rm sNANR}} = \left(\frac{p^2}{2\pi^2D^2}\right)^2\frac{1+V}{I_0\bar{S}V^2},$$

$$\mathrm{SNR}_{\upsilon^2_{\rm sNANR}} = \left(\frac{2\pi^2D^2}{p^2}\right)\frac{\sqrt{I_0\bar{S}V}\upsilon_{\rm s}^2}{\sqrt{1+V}}.$$

3.5. Noise of NANS-ASR

The noise in NANS-ASR is given as

$$\sigma^2_{\theta_{\rm NANS}} = \left(\frac{\partial\theta_{\rm NANS}}{\partial I_U^{\rm s}}\right)^2_{I_i^{\rm s}=\overline{I_U^{\rm s}}}\sigma^2_{I_U},$$

$$\sigma^2_{\theta_{\rm NANS}} = \left(\frac{p}{2\pi D}\right)^2\frac{1+V_0\sin\phi}{I_0\bar{S}V_o^2\cos^2\phi},$$

$$\mathrm{SNR}_{\theta_{\rm NANS}} = \left(\frac{2\pi D}{p}\right)\frac{\sqrt{I_0\bar{S}}\theta V_0\cos\phi}{\sqrt{1+V_0\sin\phi}}.$$

4. Simulation and discussion

In the simulation experiment, based on the wave optical approach, Matlab is used to verify the theoretical derivations. A plane wave beam of 25 keV, and phase grating (having $\pi/2$ phase shift), and absorption grating having 4 μm is used. The distance from G1 to G2 is set to be the first fractional Talbot distance, 16.13 cm. A 10-mm-dimeter PMMA cylinder is taken as sample. The refractive index of PMMA is $n = 1-4.26\times10^{-7}+{\rm i}1.53\times10^{-10}$ at 25 keV. In simulation, the projection images are acquired by ASR. To validate the theoretical expressions, the retrieved information about incident light intensity with 10^3–10^4 photons/s/mm^2 is simulated and repeated 10^4 times to calculate noise.

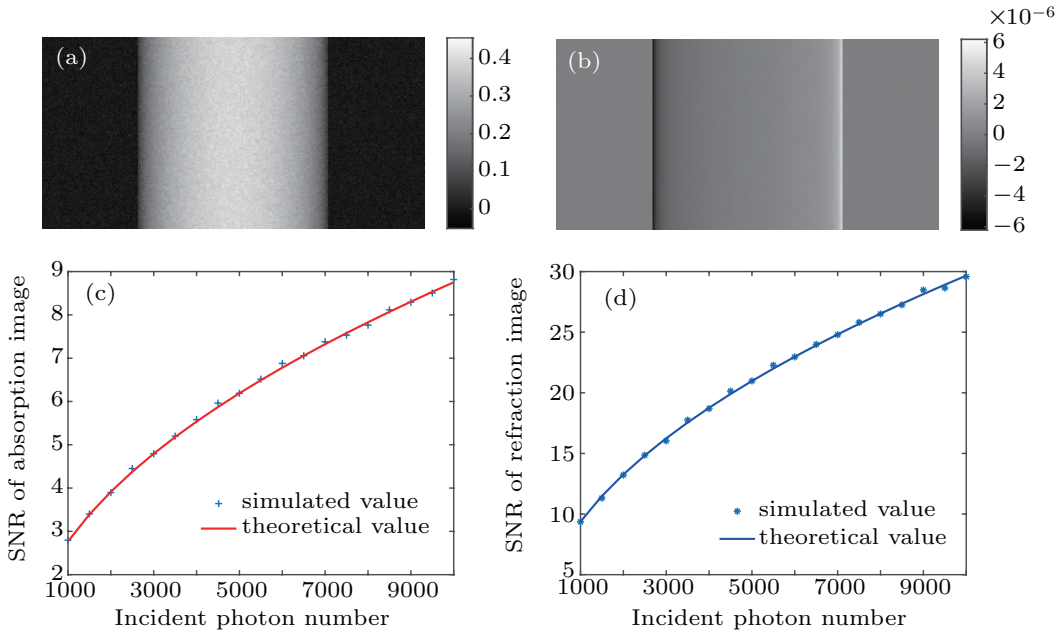


Fig. 2. (a) Absorption image, (b) refraction image, theoretical and simulated SNR of (c) absorption image and (d) refraction image *versus* incident photon number in the case of NS-ASR.

The upper panels in Fig. 2 show simulated images. Figure 2(a) shows the absorption image while figure 2(b) displays the refraction image in the case of NS-ASR. The simulated and theoretical SNR of NS-ASR are shown in lower pane of Fig. 2. Figure 2(c) shows SNRs *versus* incident photon number for absorption signal when scattering information is neglected. The SNRs *versus* incident photon for refraction image, while scattering is neglected, is shown in Fig. 2(d). Here,

it should be pointed out that in the case of NS-ASR the noise of the refraction image is higher than that of the absorption image. Therefore, the NS-ASR case can be used for investigating the samples having strong refraction properties and also for studying their edges.

Figures 3(a) and 3(b) show simulated refraction and scattering images in the case of NA-ASR, respectively. When absorption is neglected then the SNRs of refraction and scattering signals are shown in Figs. 3(c) and 3(d), respectively. It is important to note that the SNRs of refraction and scattering of NA-ASR have about the same SNRs. This case could have applications in light elements.

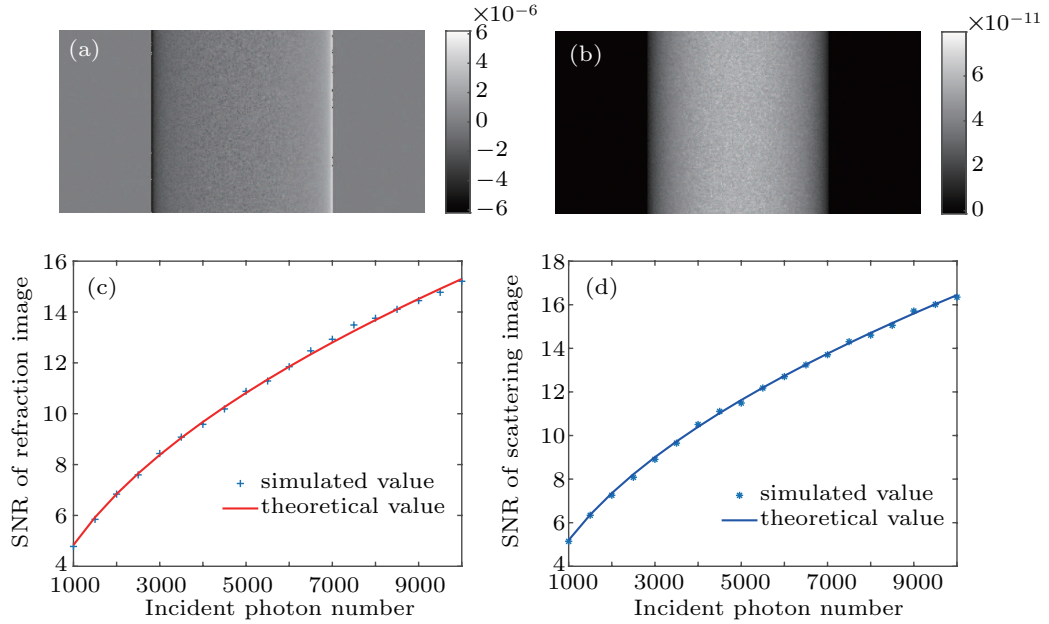


Fig. 3. Simulated (a) refraction image, (b) scattering image and simulated and theoretical SNR of (c) refraction and (d) scattering signal *versus* incident photon number in the case of NA-ASR.

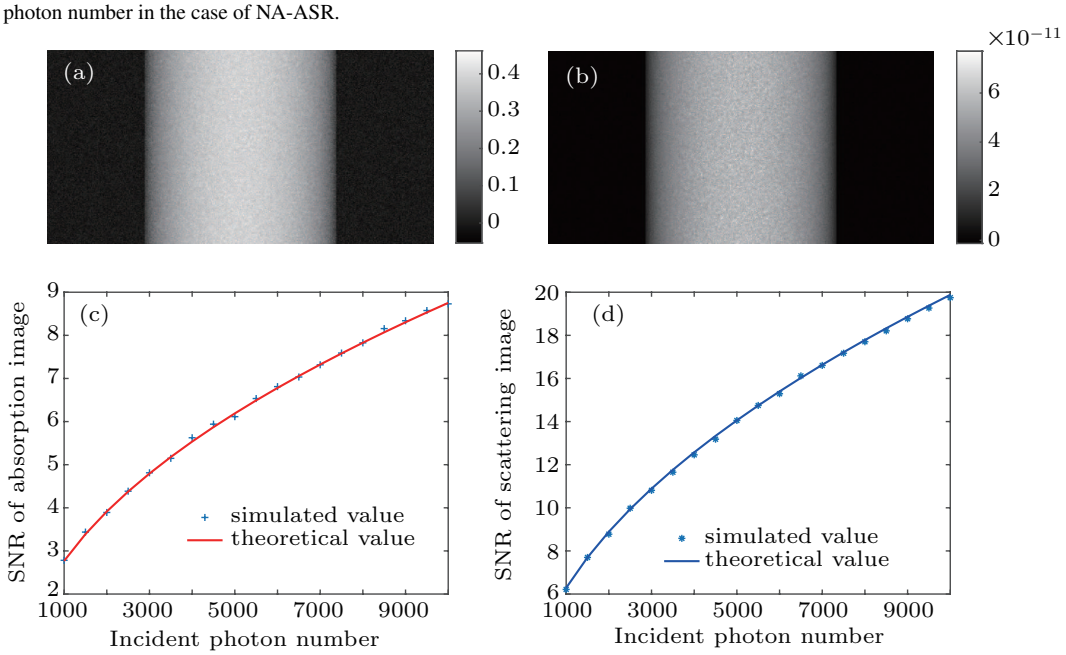


Fig. 4. Simulated (a) absorption image, (b) scattering image, and SNR of (c) absorption and (d) scattering image *versus* incident photon number in the case of NR-ASR.

The simulated absorption image and scattering image are shown in Figs. 4(a) and 4(b) while refraction is neglected. The simulated ane theoretical SNR of absorption and scattering image are shown in Figs. 4(c) and 4(d) for NR-ASR. Here, it should be pointed out that SNR of scattering image is greater than that of absorption image. NR-ASR can provide suitable image quality for soft tissues.

Figure 5(a) shows simulated scattering image in the case of NANR-ASR. The simulated and theoretical SNRs of scattering image *versus* incident photon number is shown in Fig. 5(b).

The simulated refraction image is shown in Fig. 6(a),

and the simulated and theoretical SNR *versus* incident photon number are shown in Fig. 6(b) while absorption and scattering are neglected.

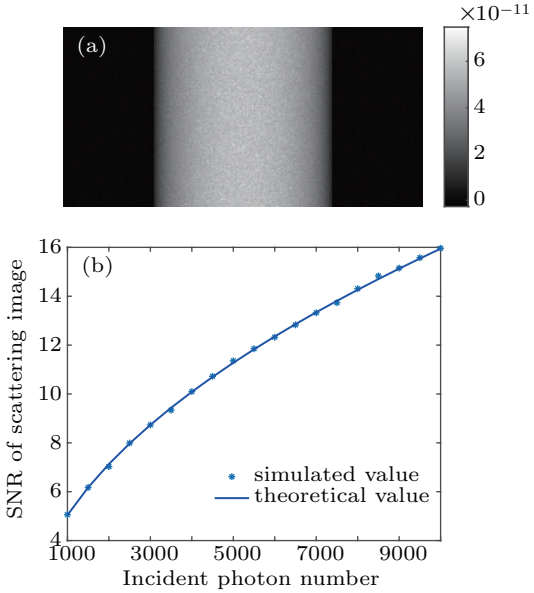


Fig. 5. (a) Simulated scattering image, and (b) simulated and theoretical SNR of scattering image *versus* incident photon number of NANR-ASR.

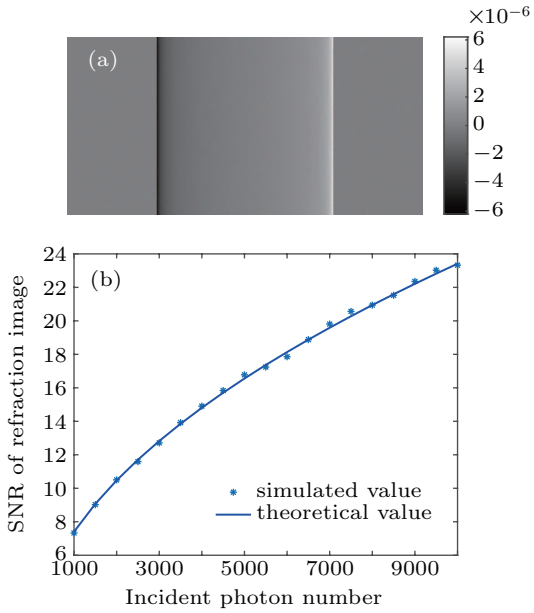


Fig. 6. (a) Simulated refraction image, and (b) simulated and theoretical SNR *versus* incident photon number in the case of NANS-ASR.

5. Conclusions

In this work, the SNRs of multi-combination images are theoretically derived for GBPCI employing ASR. The photon statistical noise, which is the main source of noise, is investigated in detail. Theoretical derivations are verified by performing simulations using Matlab. All theoretical derivations are in agreement with simulations, hence validate our theoretical derivations. The SNRs of multi-combination images (except absorption image in NS-ASR and NR-ASR) can be increased by optimizing the inter-grating distance and visibility of background SC and by reducing the grating period. The case of NS-ASR can be useful for edge enhancement and for the samples having strong refraction. While, NA-ASR could have applications in light elements. The NR-ASR case is suitable for soft elements. Finally, our SNRs of multi-combination images can provide guidelines for specific and target applications.

Appendix A: Supplementary information

In the case of negligible refraction and scattering for ASR (NRNS-ASR), only absorption information is obtained, hence the use of gratings can be omitted. This is just conventional x-ray imaging, so for completeness, we provide this information here.

When refraction and scattering are both negligible, *i.e.*, $\theta(x,y) = \upsilon_s^2(x,y) = 0$ then the absorption information can be calculated from Eq. (4) or Eq. (6) and given as

$$M_{\mathrm{NRNS}} = \ln\left[\frac{I_U^{\mathrm{b}}}{I_U^{\mathrm{s}}}\right]. \tag{A1}$$

The noise in NRNS-ASR is given as

$$\sigma^2_{M_{\mathrm{NRNS}}} = \left(\frac{\partial M_{\mathrm{NRNS}}}{\partial I_U^{\mathrm{s}}}\right)^2_{I_U^{\mathrm{s}}=\overline{I_U^{\mathrm{s}}}} \sigma^2_{I_U},$$

$$\sigma^2_{M_{\mathrm{NRNS}}} = \frac{1}{I_0\overline{S}\,\mathrm{e}^{-M}},$$

$$\mathrm{SNR}_{M_{\mathrm{NRNS}}} = \sqrt{I_0\overline{S}\,\mathrm{e}^{-M}}M.$$

The *SNR* of NRNS -ASR is independent of system parameters.

References

[1] Als-Nielsen J and McMorrow D 2011 *Elements Of Modern X-ray Physics* (New York: John Wiley & Sons)

[2] Pfeiffer F, Bech M, Bunk O, Kraft P, Eikenberry E F, Bronnimann C, Grunzweig C and David C 2008 *Nat. Mater.* **7** 134

[3] Wen H, Bennett E E, Hegedus M M and Rapacchi S 2009 *Radiology* **251** 910

[4] Yashiro W, Terui Y, Kawabata K and Momose A 2010 *Opt. Express* **18** 16890

[5] Bech M, Bunk O, Donath T, Feidenhans'l R, David C and Pfeiffer F 2010 *Phys. Med. Biol.* **55** 5529

[6] Yashiro W, Harasse S, Kawabata K, Kuwabara H, Yamazaki T and Momose A 2011 *Phys. Rev. B* **84** 094106

[7] Chen G H, Bevins N, Zambelli J and Qi Z 2010 *Opt. Express* **18** 12960

[8] Lynch S K, Pai V, Auxier J, Stein A F, Bennett E E, Kemble C K, Xiao X, Lee W K, Morgan N Y and Wen H H 2011 *Appl. Opt.* **50** 4310

[9] Modregger P, Scattarella F, Pinzer B, David C, Bellotti R and Stampanoni M 2012 *Phys. Rev. Lett.* **108** 048101

[10] Malecki A, Potdevin G and Pfeiffer F 2012 *Europhys. Lett.* **99** 48001

[11] Potdevin G, Malecki A, Biernath T, Bech M, Jensen T H, Feidenhans R, Zanette I, Weitkamp T, Kenntner J and Mohr J 2012 *Phys. Med. Biol.* **57** 3451

[12] Bao Y, Shao Q, Hu R, Wang S, Gao K, Wang Y, Tian Y and Zhu P 2016 *Radiat. Phys. Chem.* **137** 260

[13] Bonse U and Hart M 1965 *Appl. Phys. Lett.* **6** 155

[14] Momose A, Takeda T, Itai Y and Hirano K 1996 *Nat. Med.* **2** 473

[15] Nugent K, Gureyev T, Cookson D, Paganin D and Barnea Z 1996 *Phys. Rev. Lett.* **77** 2961

[16] Wilkins S, Gureyev T, Gao D, Pogany A and Stevenson A 1996 *Nature* **384** 335

[17] Davis T, Gao D, Gureyev T, Stevenson A and Wilkins S 1995 *Nature* **373** 595
[18] Chapman D, Thomlinson W, Johnston R, Washburn D, Pisano E, Gmür N, Zhong Z, Menk R, Arfelli F and Sayers D 1997 *Phys. Med. Biol.* **42** 2015
[19] Zhu P P, Wang J Y, Yuan Q X, Huang W X, Shu H, Gao B, Hu T D and Wu Z Y 2005 *Appl. Phys. Lett.* **87** 264101
[20] Zhu P, Yuan Q, Huang W, Wang J, Shu H, Chen B, Liu Y, Li E and Wu Z 2006 *J. Phys. D: Appl. Phys.* **39** 4142
[21] Pfeiffer F, Weitkamp T, Bunk O and David C 2006 *Nat. Phys.* **2** 258
[22] Weitkamp T, Diaz A, David C, Pfeiffer F, Stampanoni M, Cloetens P and Ziegler E 2005 *Opt. Express* **13** 6296
[23] Zhu P, Zhang K, Wang Z, Liu Y, Liu X, Wu Z, McDonald S A, Marone F and Stampanoni M 2010 *Proc. Natl. Acad. Sci. USA* **107** 13576
[24] Li P, Zhang K, Bao Y, Ren Y, Ju Z, Wang Y, He Q, Zhu Z, Huang W, Yuan Q and Zhu P 2016 *Opt. Express* **24** 5829
[25] Revol V, Kottler C, Kaufmann R, Straumann U and Urban C 2010 *Rev. Sci. Instrum.* **81** 073709
[26] Chen G H, Zambelli J, Li K, Bevins N and Qi Z 2011 *Med. Phys.* **38** 584
[27] Weber T, Bartl P, Durst J, Haas W, Michel T, Ritter A and Anton G 2011 *Nucl. Instrum. Method A* **648** S273
[28] Wu Z, Wang Z L, Gao K, Wang D J, Wang S H, Chen J, Chen H, Zhang K, Zhu P P and Wu Z Y 2014 *J. Electron. Spectrosc.* **196** 75
[29] Faiz W, Bao Y, Gao K, Wu Z, Wei C X, Zan G B, Zhu P P and Tian Y C 2017 *Chin. Phys. B* **26** 040602
[30] Momose A, Yashiro W, Takeda Y, Suzuki Y and Hattori T 2006 *Jpn. J. Appl. Phys.* **45** 5254
[31] Diemoz P, Coan P, Zanette I, Bravin A, Lang S, Glaser C and Weitkamp T 2011 *Opt. Express* **19** 1691
[32] Bronshtein I N and Semendyayev K A 2013 *Handbook of mathematics* (Berlin: Springer Science & Business Media)